Reinforcing Porous Silica with Carbon Nanotubes to Enhance Mechanical Performance

Jen-Tsung Luo, Hua-Chiang Wen, Chang-Pin Chou, Wen-Fa Wu and Ben-Zu Wan

Journal of Composite Materials 2007 41: 979
DOI: 10.1177/0021998306067262

Reinforcing Porous Silica with Carbon Nanotubes to Enhance Mechanical Performance

JEN-TSUNG LUO,* HUA-CHIANG WEN AND CHANG-PIN CHOU
Department of Mechanical Engineering, National Chiao Tung University Hsinchu, Taiwan

WEN-FA WU
National Nano Device Laboratories, Hsinchu, Taiwan

BEN-ZU WAN
Department of Chemical Engineering, National Taiwan University Taipei, Taiwan

ABSTRACT: In this study, porous silica (SiO_2) film is reinforced with carbon nanotubes (CNTs), which gets homogeneously dispersed in porous SiO_2 gel by ultrasonic stirring. The size of SiO_2 molecules is the same as that of nanotubes, so a fine CNTs/SiO_2 network is formed. Nanoindenters used to test the mechanical properties of the resulting specimens show a marked enhancement in the properties as a function of filler content. Interfacial bonding and the distribution of CNTs also strongly affected the mechanical performance. Although a high concentration of CNTs improves the mechanical characteristics of the matrix, it also causes agglomeration such that the mechanical performance at the surface was disproportionate. Fourier transform infrared spectroscopy (FTIR) analysis indicates that there is little chemical reaction occurring between CNTs and SiO_2. The results suggest that CNTs are ineffective reinforcements.

KEY WORDS: porous SiO_2, carbon nanotubes (CNTs), nanocomposites, mechanical properties.

INTRODUCTION

POROUS SILICA (SiO_2) of various types have great potential in applications such as integration circuit processes, microelectronic technology, environmental technology,

*Author to whom correspondence should be addressed. E-mail address: oam.me90g@nctu.edu.tw
Figures 2–6 and 9–11 appear in color online: http://jcm.sagepub.com

0021-9983/07/08 0979–13 $10.00/0 DOI: 10.1177/0021998306067262

sensors, membranes, and insulators [1–4]. The conventional porous SiO_2 was mesoporous in nature when it was first discovered in 1992 [5,6]. It is formed using surfactant micelles and liquid crystal as a template. Mesoporous SiO_2 is easily fabricated, and the pore diameters are in the range of 10–50 nm. However, the use of a high-porosity and low-polarity material and formation of inorganic material with uniform pores of arbitrary size, shape, and orientation, to improve the electrical and dielectrical properties, remains a challenge. Porous SiO_2 is of loose structure, with low mechanical strength, making further process fabrication difficult. Hence, significant interest exists in the development of methods using reinforced filler, to obtain favorable mechanical characteristics of porous SiO_2 material.

Since the first discovery of carbon nanotubes (CNTs) in 1991 [7], a new and powerful method to overcome the mechanical disadvantages of traditional materials has been developed. The CNTs are regarded as suitable composite fillers because they have excellent mechanical properties, such as high Young's modulus, excellent flexibility, low density, and high thermal conductivity.

Two main issues must be addressed to improve the mechanical properties of the composite material. They are the interfacial bonding and proper dispersion of fillers in the matrix [8,9]. According to the report, if only 1% of carbon atoms are combined with the matrix material, then the interfacial shear stress will be effectively transferred to the CNTs [10,11]. The dispersion of CNTs in the matrix is another problem to be solved. The CNT is a nanoscale material that has a giant surface area (more than 1000 m^2/g). The surface area is so enormous that van der Waal's force between any two carbon nanotubes is very strong. This force causes them to aggregate easily, which causes difficulty in dispersing CNTs in the matrix material. The homogeneous dispersion of CNTs or an exfoliation of the agglomerates and good wetting of the matrix material are considered to solve the problem of dispersion [12].

In this study, CNTs are employed as reinforcements that increase the mechanical strength of porous SiO_2 film. The solgel process is used to disperse CNTs homogeneously in a porous SiO_2 matrix. The mechanical properties, such as Young's modulus and hardness were evaluated.

EXPERIMENTAL

Multiwalled carbon nanotubes (MWCNTs), which grew from the cobalt catalyst, were synthesized from natural gas by catalytic chemical vapor deposition (CVD), with an average length of several microns, and a diameter of 10–50 nm (measured by transmission electron microscope, TEM), shown in Figure 1. The MWCNTs samples were treated by immersing them in nitric acid solution for 6 h to reduce the van der Waal's force, remove the impurities, and eliminate the metallic characteristics of the catalyst. Subsequently, samples were washed with deionized water on a filtration membrane until the acidic solution became neutral. Finally, the MWCNTs were dried in a vacuum oven at 80°C for 36 h.

The porous SiO_2 solution was prepared using Tween80 (polyoxyethylene (20) sorbitan monooleate), deionized water, ethanol (95%), hydrochloric acid (70%), and TEOS (tetraethylorthosilicate). Hydrochloric acid was used as an activating agent. Deionized water and ethanol were used as solvents. The TEOS is the precursor of SiO_2 and Tween80 is a surface-activating agent. The mixing ratio (by weight) of Tween80: deionized water: ethanol: hydrochloric acid: TEOS was 2.7 : 1 : 6 : 0.3 : 3.4. The CNTs, dispersed

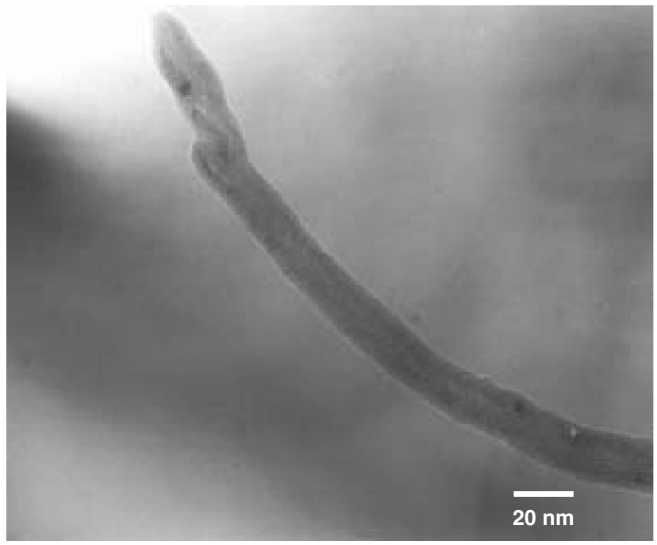

Figure 1. *TEM image of CNTs.*

in ethanol as a suspension, were added to the porous SiO_2 solution with weight fractions from 0 to 5%. The mixed CNTs/porous SiO_2 solution was stirred for 3 h at room temperature to make the solution more homogeneous. Then, the solution was spin-coated on glasses and silicon wafers. The coated samples were then soft-baked at 106°C for 1 h to solidify the mixture. Then, the film was calcined at 400°C in a furnace for 30 min to burn out the template molecules and solidify the pores. Finally, the surface was hydrophobically treated by immersing the samples in hexamethyldisilazane (HMDS) solution.

Samples from extruded composite strips were characterized using a scanning electron microscope (SEM), a transmission electron microscope (TEM), and an atomic force microscope (AFM), which yielded micrographs and surface roughness after dispersing CNTs. The nanotubes, embedded in the matrix, are invisible from the surface of the film, so the film is fractured by mechanical force or chemical etching. The fractured surface is then scanned to elucidate the microstructure. Chemical effects, such as functional groups and specific bonding characteristics were examined by FTIR analyses. The hardness and Young's modulus were measured using a nanoindenter system from nano-instruments, operated at a constant displacement rate. The stiffness was continuously measured at a small penetration depth.

RESULTS AND DISCUSSION

Figure 2 shows the AFM image of the films. It shows that the average surface roughness of the films increase from 0.34 to 1.8 nm as the weight fraction of CNT content increases from 0 to 5%. Figure 3 is the 3D magnified image of the film, with 1% CNTs, where CNTs lie on the surface. A bed-like structure of CNTs had the expected height and increased at the end point. Many researchers have found a relation between film surface morphology and electrical conductivity [13]. It is said that the nodular structure has been associated

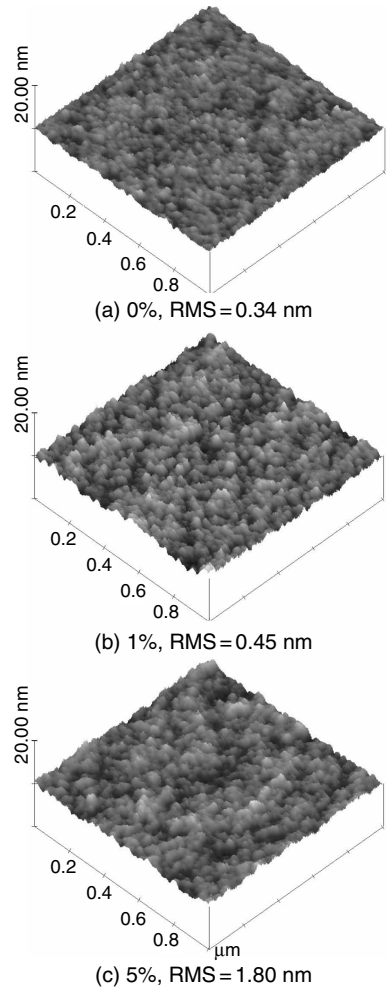

Figure 2. *AFM image of CNTs/silica film: (a) without CNT content; (b) with 1% CNTs; and (c) with 5% CNTs.*

with high-doped conducting film in which the nodules represent doping rich and highly conductive areas.

Figure 4(a) displays the SEM micrographs of cross sections of randomly oriented CNTs embedded in the porous silica matrix. Figure 4(b) presents the etching fracture surface on which some CNTs are observed. The diameter of the tubes is approximately 25 nm. Some CNTs were vertically drawn out by an extensive polishing force and integrated, as shown in Figure 4(c). Interfacial bonding between CNTs and porous SiO_2 matrix was important for the loading test. A load transfer, from the matrix to CNTs, will be effective, if the interfacial bonding is strong. The effective reinforcing modulus also strongly depends on the geometry of the filler and the combination ratio of CNTs to porous SiO_2. A bent nanotube reduces the stiffness of the composite. The constraint of the surrounding matrix on the straightening of the wavy nanotube may be significant. The geometry of wavy CNTs reduces the effective reinforcing modulus and unbent nanotubes correspond to stronger reinforcement.

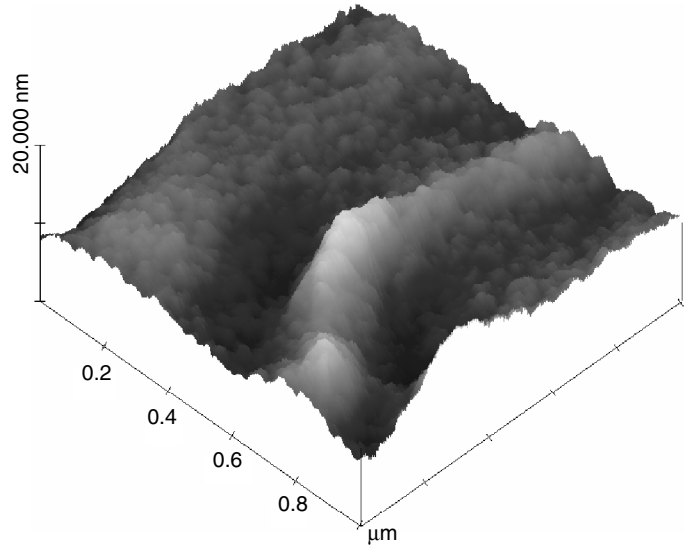

Figure 3. *Three-dimensional magnified AFM image of CNTs in porous silica matrix.*

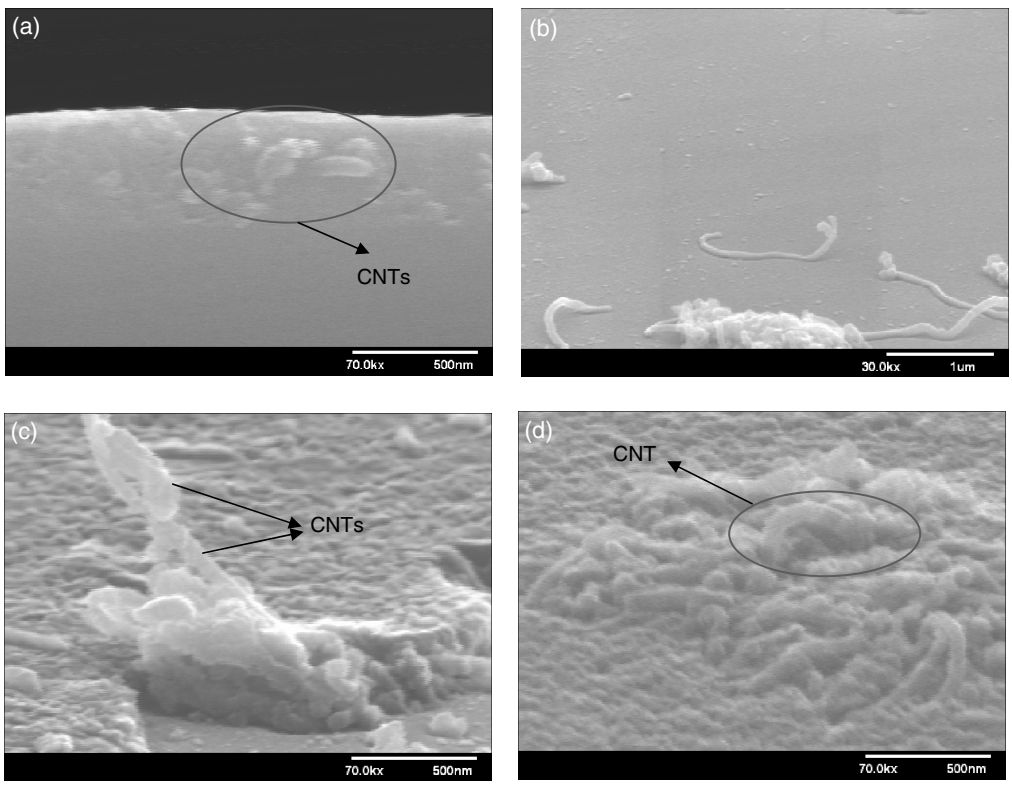

Figure 4. *SEM micrographs of CNTs/SiO_2 composites: (a) cross section image of the CNTs/SiO_2 composite; (b) etching surface of CNTs/SiO_2 composite; (c) integrated image of CNTs; and (d) aggregate image of CNTs.*

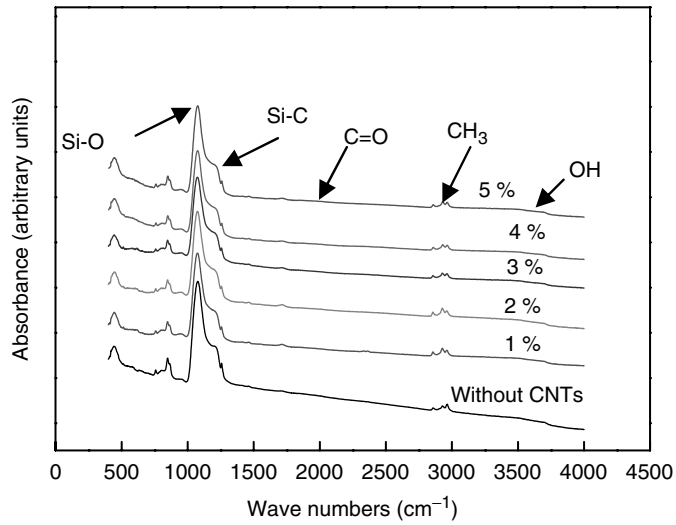

Figure 5. *FTIR spectra of porous SiO_2 film with contents of CNTs.*

The importance of a homogeneous dispersion was determined from the image of the fractured structure. The nanotubes were dispersed by sonicating them in ethanol; by mixing the suspension with porous silica resin, and evaporating the solvent. Figure 4(b) and (c) shows that some CNTs in the porous silica matrix were randomly distributed but some were agglomerated together, as presented in Figure 4(d). The agglomerate degrades the mechanical properties of the film. As reported in literatures, the agglomerate of CNTs depends on the uniformity of dispersion and size of the CNTs [14].

Figure 5 displays the results of the FTIR analysis. The FTIR spectroscopic analysis is a typical method for characterizing functional groups of CNTs/porous SiO_2 composite. The most intense absorption peak is that of SiO ($1060\,cm^{-1}$) in the main skeleton of SiO_2. This peak, centered at around $1100\,cm^{-1}$, was a shoulder at the high-frequency end of the peak at $1060\,cm^{-1}$, because the transverse optical vibration mode corresponded to the asymmetric optical stretching of the oxygen atoms in the Si-O-Si linkage [15–17]. The broad peak between 3300 and $3600\,cm^{-1}$ is related to the stretching of –OH. The hydrophobic trimethylsilyl peaks were present at 1277 and $2975\,cm^{-1}$, and are considered as SiC and CH_3. These alkyl-like groups can protect the film from attracted moisture. The mechanical performance of nanocomposite depends on the interfacial reaction between CNTs and porous silica. The atoms of Si and O are present in a strong network that is connected at short distances [18]; a loose pore structure would have a poor mechanical strength. The interfacial strength between the porous silica and the CNTs was very strong. Some C=O groups ($1700\sim1750\,cm^{-1}$), which may be carboxyl, ester, ketone, and aldehyde were found on the surface of the material. These groups take part in the polymeric reaction and enable the linkage of CNTs to the matrix, perhaps because of the mixed motion of CH_2 and COC, with deformation in inorganic silicide solution, where CH_2 is the α carbon of the matrix material and COC belongs to the CNTs. Jia et al. [19] also suggested that the π bond of CNTs may be opened and interact with the matrix. The oxidation of CNTs are responsible for reducing the amount of impurities,

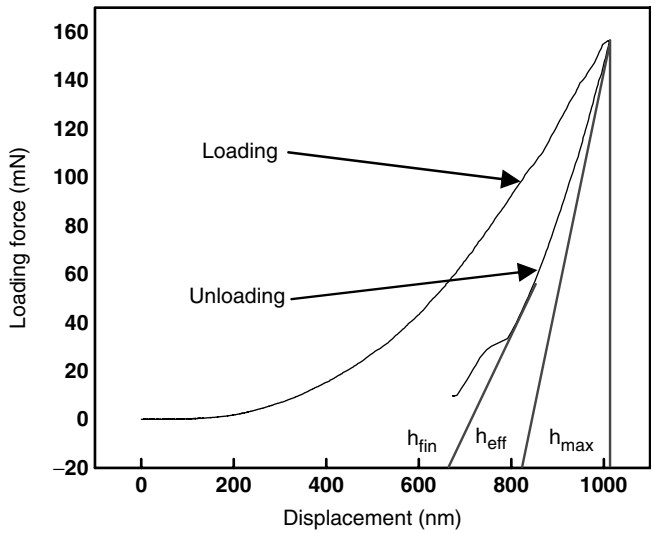

Figure 6. *Typical load vs displacement curve obtained from the nanoindenter system.*

the factor which may also contribute to the interaction between the CNTs and the silica matrix. However, C=O groups may also be regarded as an oxidation product of ethanol which is used as a solvent. The presence of C=O resulted in a polar surface and caused a chemical change.

The mechanical properties, such as hardness and Young's modulus, were tested using a nanoindenter system. They were obtained from load–displacement data, with penetration depths of 1/10 of the thickness of the film, to avoid surface and substrate damage [20–23]. Figure 6 plots the typical load–displacement curve obtained from the nanoindenter system. The indenter is a triangular pyramid-shaped diamond with a shape angle of 115°. Every sample was tested 10 times at different locations of the surface. The Young's modulus and hardness were average values. Equation (1) yields the indentation depth, with the given pyramidal geometry, from the diagonal length of the indentation (l_p).

$$h_p = \frac{l_p\sqrt{3 - \tan^2(\theta/2)}}{3\tan(\theta/2)} \tag{1}$$

where θ is the edge angle of the indenter, l_p is the diagonal length of the indentation, and h_p is the penetration depth. The surface area must be determined to measure the surface hardness, which equals the mean pressure under the indenter. The length of the diagonal of the indentation must be measured to determine the surface area.

$$S_p = \frac{9h^2\tan(\theta/2)}{3 - \tan^2(\theta/2)}. \tag{2}$$

Equation (2) yields the surface area (S_p) for a given pyramidal geometry. The plastic depth can be determined from the penetration depth using h_{eff} as the plastic depth, which is

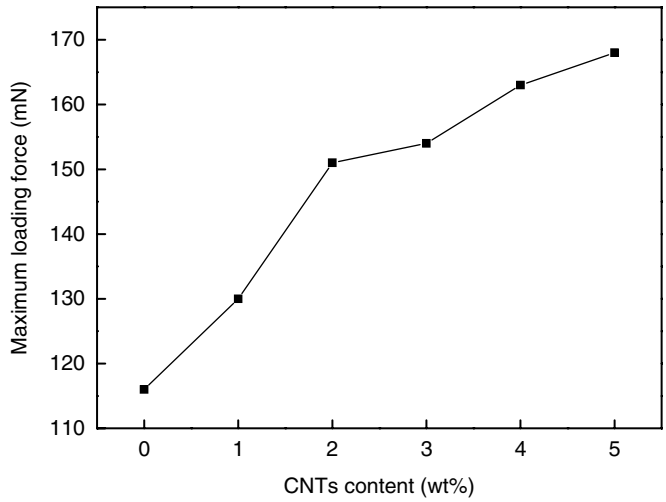

Figure 7. *Maximum loading of different CNT contents on the CNTs/SiO_2 composite.*

associated with the point of intersection between the sloping line of the maximum load point and the x-axis, and is measured by the method of least squares [24]. The h_{fin} is the position where the indenter was detached from the surface of the sample. The $h_{\max}$ is the position at which the indenter touches the sample's maximum depth. Figure 6 presents the values of the aforementioned parameters.

Figure 7 plots the maximum loading force versus CNT content of the samples. The maximum loading force increased with CNT content, reaching 168 mN at a CNT weight fraction of up to 5%. The load force, without the CNT sample, was only about 116 mN. It cannot be regarded as an elastic or plastic modulus when the part of the curve from which the average gradient was determined involves both elastic and plastic deformation. However, the maximum load corresponded to a combination of the resistance of the material to the deformation before and after yielding. This value is also related to the yield strength of the material, because this value marks the transition between the maximum values of the load during the penetration depth experiment. This is a measure of the capacity of the material to absorb energy before breaking [25,26]. The result also indicated that this property is related to the wear resistance of a class of porous SiO_2, including fillers. Figure 7 clearly shows that the addition of CNTs changed the mechanical characteristics of porous SiO_2.

Figure 8 presents the relationship between load and hardness. All of the samples considered herein were prepared under the same conditions, except for the CNT content. Hence, the hardness curve is assumed to be caused by the change in CNT content. The hardness increased with the penetration load. When the nanoindenter test is performed with a small load, the area of the sphere at the tip of the indenter is not negligible. The hardness of the composite was also shown to be a function of the filler content. The hardness curves at CNT contents of 1–3% are similar and the curves at CNT contents between 4 and 5% are also similar. Accordingly, a step-region threshold concentration of the filler may be considered to exist. When the filler content exceeded this threshold concentration, the mechanical performance of the matrix was substantially higher. The higher CNT content in porous silica film corresponds to

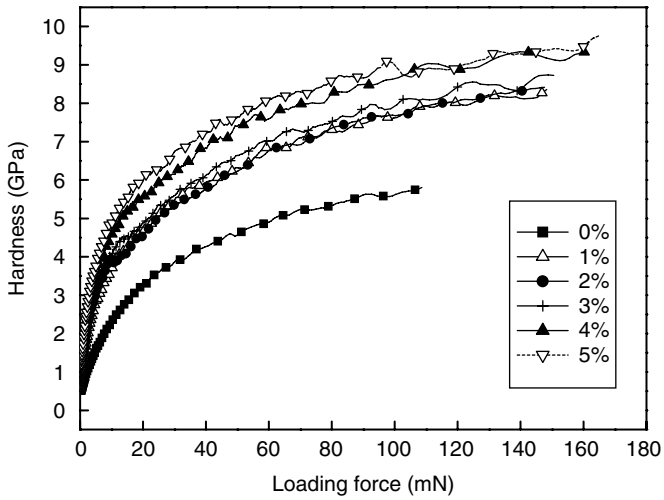

Figure 8. *Hardness vs loading curve of CNTs with different weight contents on the CNTs/SiO_2 composite.*

greater hardness, because more CNT interacts with SiO_2 molecules, strengthening the transfer of loading.

The contact stiffness must be obtained from the gradient of the unload curve to find the effective Young's modulus [27]. The effective Young's modulus is related to the stiffness and given by Equation (3).

$$S = \frac{dP}{dh} = C_A E^* \sqrt{A_r} \tag{3}$$

where

$$\frac{1}{E^*} = \frac{1-\upsilon_1^2}{E_1} + \frac{1-\upsilon_s^2}{E_s}$$

where E^* is the reduced modulus; C_A equals $2/\sqrt{\pi}$, and A_r is the projected real contact area between indenter and surface. E_1 and ν_1 are the Young's modulus and the Poisson's ratio of the indenter. E_s and ν_s are the corresponding parameters of the test sample. S represents the contact stiffness. When the nanoindentation test is undertaken with the triangular pyramidal indenter with a shape angle of $\theta = 115^\circ$, the constant (C_A) must be $2/\sqrt{\pi}$.

When the indenter tip penetrated the composites, the loading force was significantly dispersed by the large quantity of CNTs. Figure 9 plots Young's modulus versus displacement. The modulus increases with the displacement. The gradient of Young's modulus declines at shallow depths, until a contact depth of 320 nm is reached. The curve suggests that the sample with CNT fillers is stiffer than that without fillers. If the surface layer, without CNTs fillers, undergoes elastic deformation, then plastic deformation will occur. The similar plot of hardness versus displacement (Figure 10) shows analogous behavior as in Figure 9.

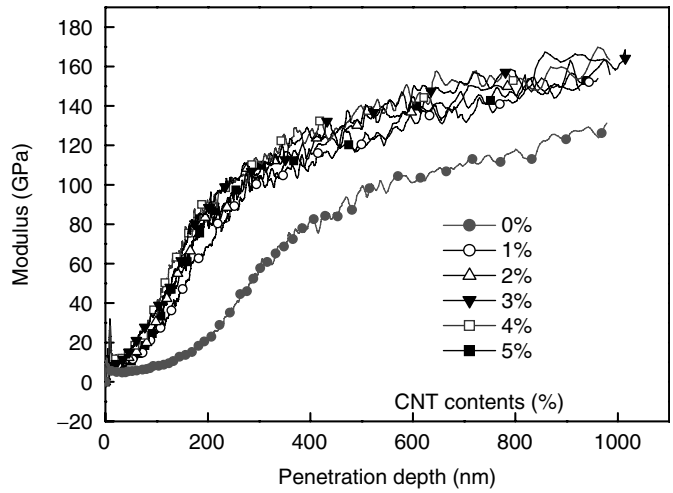

Figure 9. *Modulus vs displacement curve of CNTs with different weight contents on the CNTs/SiO_2 composite.*

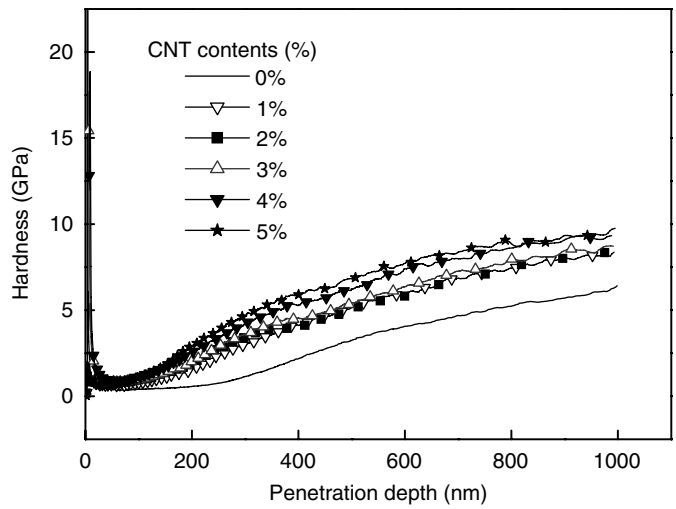

Figure 10. *Hardness vs displacement curve of CNTs with different contents on the CNTs/SiO_2 composite.*

The effective modulus of the CNTs/porous SiO_2 composite is related to the weight fraction of CNTs. Figure 11 plots the hardness and Young's modulus of the composites as functions of the weight fraction of CNTs from 1 to 5%. At a CNT content of 1%, the Young's modulus was about four times larger than that of the unreinforced sample, and increased with CNT content. The dependence of Young's modulus on the nanotube weight fraction is associated with the effect of load transfer from the matrix to CNTs, which have a large aspect ratio and excellent mechanical properties. The effective distribution of CNTs in the surrounding matrix at low content also contributes to this dependence. If CNTs are dispersed uniformly in the matrix, the effective load transfer

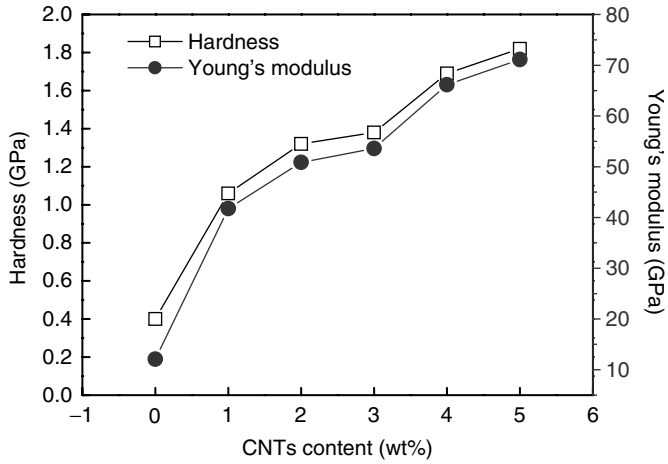

Figure 11. *Effect of CNT content on the hardness and Young's modulus of CNTs/SiO_2 composite.*

from the matrix to CNTs is very enormous. Load sharing between the CNTs and matrix enhances the mechanical properties of the composite. The results also demonstrate that CNT-reinforced polymer or alumina composite are stronger than other fillers [28,29]. However, higher CNT contents of over 10% resulted in the agglomeration of CNTs in the surrounding matrix, and suppressed densification. A high fraction of nanotubes also caused the deflection of cracks and continuous crack propagation [30]. It also degraded the mechanical properties. Additionally, sintering impurities may promote the crystallization of SiO_2 by heterogeneous nucleation [31].

CONCLUSION

Different weight fractions of CNTs and porous SiO_2 films were produced. The CNTs were homogeneously dispersed into porous silica solgel using a sonication method. A functional nanotube which does not interact chemically with porous SiO_2 expresses itself in the presence of agglomerates. The hardness and Young's modulus of CNTs/porous SiO_2 composites were enhanced with the increase of CNT content. It was due to the load transfer between the CNTs and porous silica from interfacial bonding. However, higher CNT content made CNTs agglomerate together and degraded the mechanical performance. The method presented in this study provides a means for parametrically exploring the reinforcement–matrix relationships. Further improvement should optimize the process of procedure to enhance the reinforcing role of CNTs.

ACKNOWLEDGMENT

The authors would like to thank the National Science Council of the Republic of China, Taiwan, for financially supporting this research under Contract No. NSC 94-2216-E-009-027.

REFERENCES

1. Wang, Y.H., Moitreyee, M.R., Kumar, R., Wu, S.Y., Xie, J.L., Yew, P., Subramanian, B., Shen, L. and Zeng, K.Y. (2004). The Mechanical Properties of Ultra-low-dielectric-constant Films, *Thin Solid Films*, **462–463**: 227.
2. Sugahara, G., Aoi, N., Kubo, M., Arai, K. and Sawada, K. (1997). Nano-scale Structure Control of Mesoporous Silica, In: *Proceedings of the Third International Dielectrics for ULSI Multilevel InterconnectionConference*, Santa Clara, CA, USA February (1997), p. 19.
3. Martin, S.J., Goldschalx, J.P., Mills, M.E., Shaffer II, E.O. and Townsend, P.H. (2000). Development of a Low-dielectric-constant Polymer for the Fabrication of Integrated Circuit Interconnect, *Adv. Mater.*, **12**: 1769.
4. Morgen, M., Ryan, E.T., Zhao, J.H., Hu, C., Cho, T.H. and Ho, P.S. (2000). Pore Size and Pore-size Distribution Control of Porous Silica, *Annu. Rev. Mater. Sci.*, **30**: 645.
5. Kresge, C.T., Leonowicz, M.E. and Roth, W.J. (1992). Ordered Mesoporous Molecular Sieves Synthesized by a Liquid-crystal Template Mechanism, *Nature*, **359**: 710.
6. Beck, J.S. and Vartuli, J.C. (1992). A New Family of Mesoporous Molecular Sieves Prepared with Liquid Crystal Templates, *J. Am. Chem. Soc.*, **114**: 10834.
7. Iijima, S. (1991). Pentagons, Heptagons and Negative Curvature in Graphite Microtubule Growth, *Nature*, **354**: 56.
8. Cooper, C.A., Cohen, S.R., Barber, A.H. and Wagner, H.D. (2002). Detachment of Nanotubes from a Polymer Matrix, *Appl. Phys. Lett.*, **81**: 3873.
9. Lu, K.L., Lago, M., Chen, Y.K., Green, M.L.H., Harris, P.J.F. and Tsang, S.C. (1996). Mechanical Damage of Carbon Nanotubes by Ultrasound, *Carbon*, **34**: 814.
10. Shelimov, K.B., Esenaliev, R.O., Rinzler, A.G., Huffman, C.B. and Smalley, R.E. (2004). Carbon Nanotube-reinforced Epoxy-composites: Enhanced Stiffness and Fracture Toughness at Low Nanotube Content, *Compos. Sci. Technol.*, **64**: 2363.
11. Frankland, S.J.V., Caglar, A., Brenner, D.W. and Griebel, M. (2002). Molecular Simulation of the Influence of Chemical Cross-Links on the Shear Strength of Carbon Nanotube-Polymer Interfaces, *J. Phys. Chem. B*, **106**: 3046.
12. Zhang, M., Yudasaka, M., Koshio, A. and Iijima, S. (2001). Effect of Polymer and Solvent on Purification and Cutting of Single-wall Carbon Nanotubes, *Chem. Phys. Lett.*, **349**: 25.
13. Barishi, J.N., Stella, R., Spinks, G.M. and Wallace, G.G. (2000). Carbon Nanotubes with Single-layer Walls, *Electrochim. Acta.*, **46**(4): 519.
14. Liu, W., Hoa, S.V. and Pugh, M. (July 2003). Effect of Carbon Nanotube Addition on the Tribological Behavior of Carbon/Carbon Composites, In: *Proceedings of 14th International Conference on Composite Materials, ICCM-14*, San Diego, CA, July (2003), Paper ID 1407.
15. Yu, S., Wong, T.K.S., Pita, K., Hu, X. and Ligatchev, V. (2002). Skeletal Silica Characterization in Porous-silica Low-dielectric-constant Films by Infrared Spectroscopic Ellipsometry, *J. Appl. Phys.*, **92**: 333.
16. Gorman, B.P., Rosa, A. and Mueller, D.W. (2001). High Strength, Low Dielectric Constant Fluorinated Silica Xerogel Films, *Appl. Phys. Lett.*, **79**: 4010.
17. Lim, S.W., Shimogaki, Y., Nakano, Y., Tada, K. and Komiyama, H. (1996). Preparation of Low-Dielectric-Constant F-Doped SiO_2 Films by Plasma-Enhanced Chemical Vapor Deposition, *Jpn. J. Appl. Phys.*, **35**: 1468.
18. Han, Y.S., Li, J.B., Wei, Q.M. and Wen, Z.H. (2003). The Effect of SiO_2 Addition on Porous Silica Composite Strength, *Mater. Lett.*, **57**: 3847.
19. Jia, Z., Wang, Z., Xu, C., Liang, J., Wei, B., Wu, D. and Zhu, S. (1999). Study on Poly(methyl methacrylate)/carbon Nanotube Composites, *Mater. Sci. Eng.*, **A271**: 395.
20. Shen, L. and Zeng, K.Y. (2004). Comparison of Mechanical Properties of Porous and Non-porous Low-k Dielectric Films, *Microelectron. Eng.*, **71**: 221.
21. Shen, L., Zeng, K.Y., Wang, Y.H., Narayanan, B. and Kumar, R. (2003). Determination of the Hardness and Elastic Modulus of Low-k Thin Films and their Barrier Layer for Microelectronic Applications, *Microelectron. Eng.*, **70**: 115.

22. Nay, R.J., Warren, O.L., Yang, D. and Wyrobek, T.J. (2004). Mechanical Characterization of Low-k Dielectric Materials using Nanoindentation, *Microelectron. Eng.*, **75**: 103.
23. Li, X., Bhushan, B., Takashima, K., Baek, C.W. and Kim, Y.K. (2003). Mechanical Characterization of Micro/Nanoscale Structures for MEMS/NEMS Applications using Nanoindentation Techniques, *Ultramicroscopy*, **97**: 481.
24. Doener, M.F. and Nix, W.D. (1986). On the Axial and Interfacial Shear Stresses due to Thermal Mismatch in Hybrid Composite Sheets, *J. Mater. Res.*, **1**: 601.
25. Edidin, A.A. and Kurtz, S.M. (2001). Model Experiment on a Protrusion Method for Measurement of Interface Shear Sliding Stress in Fiber-reinforced Composite, *Funct. Biomater.*, **198**: 1.
26. Mao, X., Saito, M. and Takahahi, H. (1987). A New Look at Shear Correction Factors and Warping Functions of Anisotropic Laminates, *Scripta Metal Mater.*, **25**: 2481.
27. Fukuhara, M. and Yamauchi, I. (1993). Effect of Indenter Tip Radius on the Load Deflection Behavior of Thin Plates, *J. Mater. Sci.*, **28**: 4681.
28. Odegard, G.M., Gates, T.S., Wise, K.E., Park, C. and Siochi, E.J. (2003). Constitutive Modeling of Nanotube-reinforced Polymer Composites, *Compos. Sci. Technol.*, **63**: 1671.
29. Mo, C.B., Cha, S.I., Kim, K.T., Lee, K.H. and Hong, S.H. (2005). Fabrication of Carbon Nanotube Reinforced Alumina Matrix Nanocomposite by Sol–Gel Process, *Mater. Sci. Eng. A*, **395**: 124.
30. Liao, Y.H., Olivier, M.T., Liang, Z., Zhang, C. and Wang, B. (2004). Investigation of the Dispersion Process of SWNTs/SC-15 Epoxy Resin Nanocomposites, *Mater. Sci. Eng. A*, **385**: 175.
31. Peter, P.B. (1983). Stress Distribution along Broken Fibres in Polymer-matrix Composites, *J. Am. Ceram. Soc.*, **66**: C188.